Formation Mechanisms of Self-Organized Needles in Porous Silicon Based Needle-Like Surfaces

Formation Mechanisms of Self-Organized Needles in Porous Silicon Based Needle-Like Surfaces

Shervin Keshavarzi,[1,2,z] Ulrich Mescheder,[2] and Holger Reinecke[1,3]

[1] *Department of Microsystems Engineering-IMTEK, Freiburg University, Freiburg 79110, Germany*
[2] *Department of Medical and Mechanical Engineering, Furtwangen University, Institute for Microsystems Technology-IMST, Furtwangen 78120, Germany*
[3] *Schölly Fiberoptic GmbH, Denzlingen 79211, Germany*

Formation mechanisms of self-organized Si-needles generated by anodic etching of lowly doped p-type silicon wafers in an aqueous HF solution in the transition region (region between the pore formation and the electropolishing) is studied through surface SEM images taken after different etch times. Impacts of current density, substrate resistivity range in the lowly doped region, and electrolyte additives on morphology of needles are also investigated. A simple model based on pore formation models is presented to describe formation of self-organized needles during anodic etching of lowly doped p-type silicon in an aqueous HF solution in the transition region. The validity of the model is discussed by comparison to experimental results.
 [DOI: 10.1149/2.0501803jes]

Manuscript submitted December 5, 2017; revised manuscript received January 30, 2018. Published February 21, 2018. This was Paper 1017 presented at the National Harbor, Maryland Meeting of the Society, October 1–5, 2017.

Anodization is a well-known technique for porous silicon (PSi) formation or electropolishing of silicon (Si) wafers. Although the technique is known for several decades, it has attracted renewed interest since 1990 resulting from discovery of luminescence properties of PSi.[1] The technique has also emerged in micromachining due to its low cost, easy implementation, and compatibility with standard microelectronic processes.[2] Usage of the anodization technique to create needle-like Si surfaces for room temperature Si-Si bonding applications has currently attracted attention.[3–5] Additionally, the technique has a good potential to easily replace complicated and costly processes, such as inductively coupled plasma reactive ion etching (ICP-RIE),[6] interference lithography combined with Reactive Ion Etching (RIE) technique,[7] metal-assisted etching (MAE) technique,[8] and laser micro/nano-processing,[9] which are commonly used to generate Si needle-like antireflection coating surfaces for visible and (near infrared) NIR applications.

Using the anodization technique, needle-like surfaces can be obtained by anodic etching of lowly doped p-type Si in aqueous HF solutions in the so-called transition region, the region between pore formation and electropolishing.[3–5] Although formation of PSi and electropolishing of p-type Si are quite well-understood, formation mechanisms of self-organized needles in the transition region, where both pore formation and electropolishing are competing for control over the surface,[10] is still unclear since instabilities in space and time are occurring in this region.[11] Even though formation mechanisms of needles generated by anodization of p-type Si are briefly described in,[12,13] no model for their formations has been reported yet. In this work, formation mechanisms of self-organized needles generated by anodic etching of lowly doped ($<10^{15}$ atoms/cm^3)[14] p-type Si in an aqueous HF solution is investigated in detail. Impacts of current density and substrate resistivity range in the lowly doped region, and electrolyte additives on morphology of surfaces are also discussed. A simple model based on the Current Burst (CB) model,[15] the Zhang model (distribution of the electric field at different regions of a pore),[16] and the Lehmann macro-pore formation model[17] is then presented to describe formation of needles in the transition region.

Experimental

Current density-voltage characteristic.—Anodic current density-voltage (*J-V*) characteristic of the Si-electrolyte interface for a quarter of a lowly boron doped (12–17 Ωcm) CZ 4-inch <100> p-Si wafer with a circular anodization aperture with an area of 5.7 cm^2 and back side sheet resistance of 16 ± 0.3 Ω/□ (achieved by the thermal diffusion method) in a 7.2 wt% aqueous HF solution (see Fig. 1) was obtained through the linear sweep voltammetry method using a potentiostat (Bio Logic SP-150) with scanning rate of 100 mV/s. For this purpose, a tiny cylindrical platinum (Pt) reference electrode (with radius of R = 250 µm and length of L = 5 mm) was positioned 2 mm away from the Si surface in a double tank cell. Positions of current peaks (J_{PS}: below which pore formation occurs and J_{El}: above which electropolishing occurs) on the obtained *J-V* curve were then used to find the pore formation region, the transition region, and the electropolishing region in relation to the current density for this specific condition.[16]

Similar wafers were then anodized with the same condition for a fixed anodization time of 40 minutes with different constant current densities in a range of 30–70 mA/cm^2 to verify these regions. Figure 2 shows generated surfaces, which dried through ethanol and then pentane for 15 minutes each to reduce capillary effect and induced stress on surfaces. The constant current density of 30 mA/cm^2 resulted in two PS layers (see Fig. 2a), a layer with large pores in the µm range (macro-pores) covered by another layer with much smaller pore size (micro/meso-pores). The micro/meso-pores layer had entirely cracked

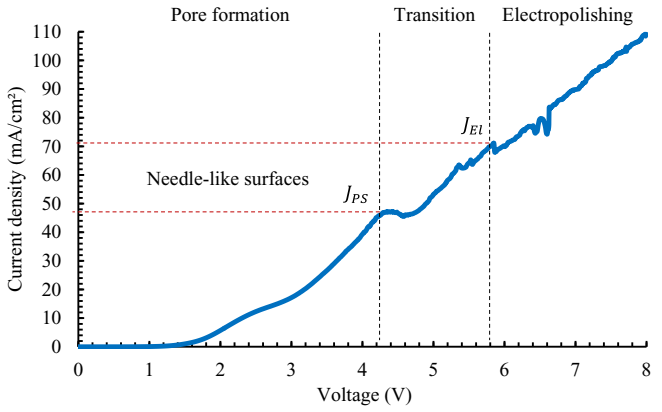

Figure 1. Measured J-V curve of a quarter of 4-inch <100> CZ 12–17 Ωcm p-type Si wafer with a circular anodization aperture with an area of 5.7 cm^2 in a 7.2 wt% aqueous HF solution.

[z] E-mail: kesh@hs-furtwangen.de

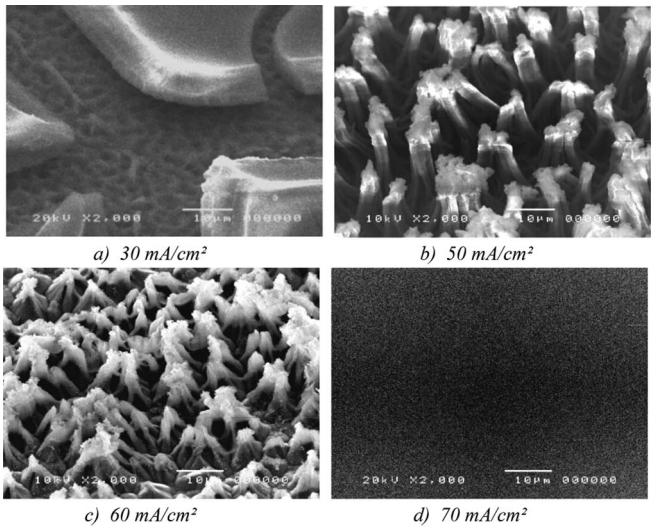

Figure 2. SEM images of surfaces anodized with different constant current densities in a 7.2 wt% aqueous HF solution for a duration of 40 minutes using quarters of a 4-inch <100> CZ 12–17 Ωcm p-type Si wafer.

and broken to smaller pieces because of the large capillary stress induced on the surface due to its high porosity and thickness.[18] Current densities of 50 mA/cm^2 and 60 mA/cm^2 resulted in needle-like surfaces with different morphologies (see Figs. 2b and 2c) in which single needles stuck together at the top forming clusters of needles. Due to stochastic nature of pore geometries and morphologies[14] and clustering behavior of needles, clustered needles with inhomogeneous length, diameter, and separation were obtained. However, current density of 70 mA/cm^2 resulted in complete electropolishing of the surface (see Fig. 2d). Positions of current density peaks (J_{PS} and J_{EI}) on the obtained *J-V* curve (see Fig. 1) and morphology of generated surfaces (see Fig. 2) were clearly indicating and confirming generation of self-organized needle-like surfaces in the transition region.

Formation mechanisms of needles.—Formation mechanisms of needles were monitored by taking surface SEM images after different etch times during anodization of similar wafers (<100> CZ 12–17 Ωcm p-type Si) with a constant current density of 50 mA/cm^2 in a 7.2 wt% aqueous HF solution. For this purpose, three wafers were cut into twelve quarters, and each quarter was anodized for different durations between 1 and 40 minutes. Top-view SEM images of surfaces obtained at various etch times are shown in Figure 3. A slight inhomogeneous dissolution was occurring at the beginning of the process prior to pores initiations (see Fig. 3a). Initiation of needles was starting by nucleation of pores, where the surface was roughened and pitted due to inhomogeneous etching of Si (see Fig. 3b). Ununiform dissolution of the surface was resulting in random creation of irregular islets with varied sizes and heights (see Fig. 3c). With increasing time, small and short islets were etched away, and new larger size islets were generated instead (see Fig. 3d). Further etching of the surface reformed shapes of large irregular islets to pyramid-shape islets by slightly narrowing their side walls and increasing their heights (see Figs. 3e and 3f and Fig. 4). As the time increased, side walls of pyramid-shape islets were narrowed more, and their heights were increased further (Fig. 3g and Fig. 4). Further etching of side walls was resulting in formation of semi-cylindrical needles in which their tips were attached together and made clusters of needles (see Fig. 3h). At this stage, with increasing time, only lengths of needles were increased, and no significant reduction in diameter of needles were observed (see Fig. 3i and Fig. 4). Some of these characteristics can be clearly seen from height information of formed structures (asperities, irregular islets, pyramid-shape islets, and clustered needles) during

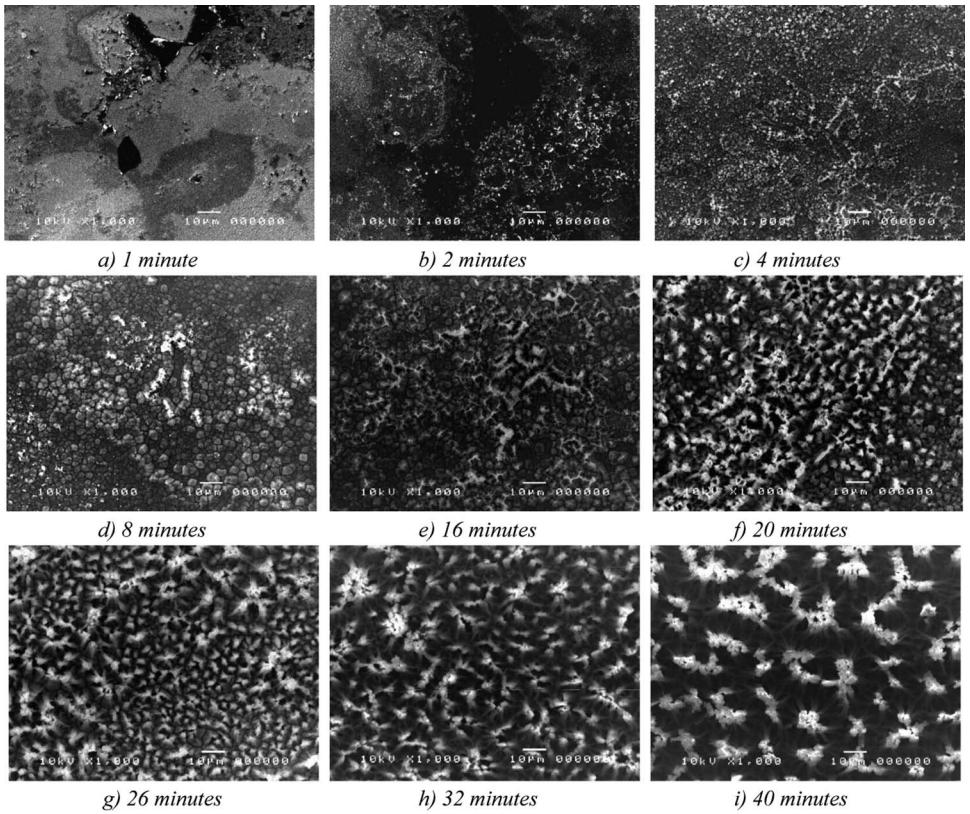

Figure 3. Top-view SEM images showing formation mechanisms of needles during anodic etching of <100> CZ 12–17 Ωcm p-type Si wafers at different etching times in a 7.2 wt% aqueous HF solution with a constant current density of 50 mA/cm^2.

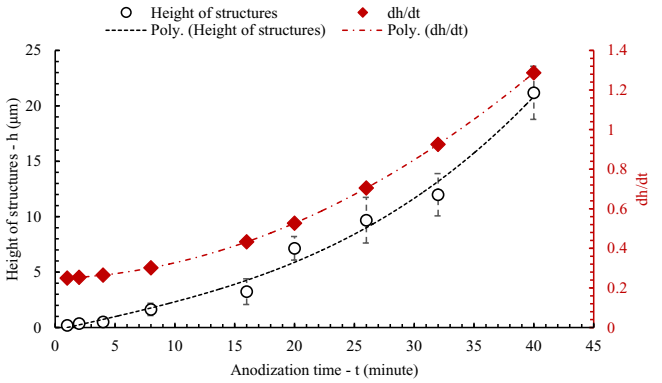

Figure 4. Measured height of formed structures (asperities, irregular islets, pyramid-shape islets, and clustered needles) and its first derivate in respect to etching time (dh/dt) as a function of anodization time.

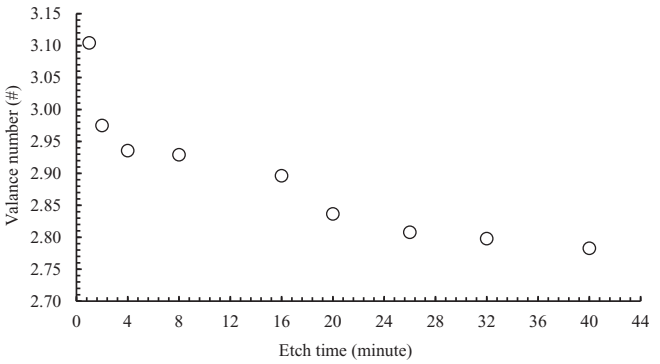

Figure 5. Calculated average dissolution valence number as a function of anodization time for <100> CZ 12–17 Ωcm p-type Si wafers anodized in a 7.2 wt% aqueous HF solution with a constant current density of 50 mA/cm^2.

the 40 minutes anodization (see Fig. 4). Height of structures is nonlinearly increasing by increasing etching time. Assuming a constant etch rate over a time and dividing etching, which occur at a time into two components: "planar etching" responsible for surface area etching and "vertical etching" responsible for depth etching, the vertical etch rate (first derivate of height of formed structures over anodization time (dh/dt)) is nonlinearly increasing with increasing etching time. The vertical etch rate is slowly increasing at the beginning of the process (between time 1 to 8 minutes) and raising faster (with higher slop) by formation of large islets (between time 8 to 40 minutes).

The average dissolution valence (n_v) of the chemical reaction between Si and the electrolyte (the ratio of exchanged charge carriers per dissolved silicon atom during the etching process) during 40 minutes anodization can be calculated through:[19]

$$n_v = \frac{I \times t \times m_{Si}}{e \times \Delta_m} \qquad [1]$$

where I is the applied current (A), t is the anodization time (s), Δ_m is the dissolved mass of Si (mg), $e = 1.602 \times 10^{-19}$ C is the elementary charge, and $m_{Si} = 4.6637 \times 10^{-23}$g is the atomic mass of silicon.

The average dissolution valence calculated from experimental results is nonlinearly decreasing from $n_v = 3.11$ for the short anodization time (1 minute) to $n_v = 2.78$ for the long anodization time (40 minutes) during the anodization process as it is shown in Figure 5. This indicates that the indirect dissolution of silicon via oxide formation (see reactions described by Eqs. 3 and 4) is almost dominant at the beginning of the process; however, with increasing time, the direct dissolution (see the reaction described by Eq. 2) becomes more dominant.

Impact of current density on morphology of needle-like surfaces.—4-inch <100> CZ 10–20 Ωcm p-type Si wafers with back side sheet resistances of 18.3 ± 0.5 Ω/□ were anodized in a 7.2 wt% HF aqueous solution with various constant current densities (45–55 mA/cm^2) in the transition range for a duration of 40 minutes to study the impact of current density on morphology of needle-like surfaces and geometrical properties of needles. Generated needle-like surfaces (see Fig. 6) were dried through ethanol and then pentane for 15 minutes each. Single needles were typically stuck together at the top forming clusters of needles through a self-attaching mechanism, due to either strongly induced capillary forces between them during rinsing and drying processes or their formation process.[5] Due to nonuniformity of pores pitches and sizes, configurations of macro-pores,[12] and clustering behavior of needles, clustered needles with inhomogeneous lengths, diameter, and separation were obtained. Morphology of needle-like surfaces was investigated through surface SEM images. Geometries of clustered needles, such as clustered needle density, diameter of clustered needles, length of clustered needles, and distance between adjacent clustered needles were extracted using SEM images (see Fig. 7). The clustered needle density and length of clustered needles increased by increasing the current density. The distance between adjacent clustered needles decreased by increasing the current density. The diameter of clustered needles showed a slight decrement in respect to increasing current density.

Impact of substrate resistivity on morphology of needle-like surfaces.—An aqueous electrolyte with 7.2 wt% HF at temperature of 21°C, a constant current density of 50 mA/cm^2, and an anodization time of 40 minutes were considered as the starting condition to study the impact of the wafer resistivity on morphology of needle-like surfaces. Full 4-inch CZ <100> p-type Si wafers with various resistivity ranges (1–5 Ωcm, 5–10 Ωcm, 10–15 Ωcm, 15–20 Ωcm, 20–25 Ωcm, and 25–30 Ωcm) in the lowly doped range (<10^{15} atoms/cm^3) were anodized with above parameters. Figure 8 shows SEM surface images of generated surfaces. Specific morphologies of obtained surfaces and their homogeneities at this specific process condition were sensitively dependent on resistivity of the wafer. Needle-like surfaces obtained only from the 10–15 Ωcm wafer and the 15–20 Ωcm wafer. Needles obtained from the 10–15 Ωcm wafer stuck together at the top and made clusters of needles (Fig. 3b); whereas clusters needles obtained

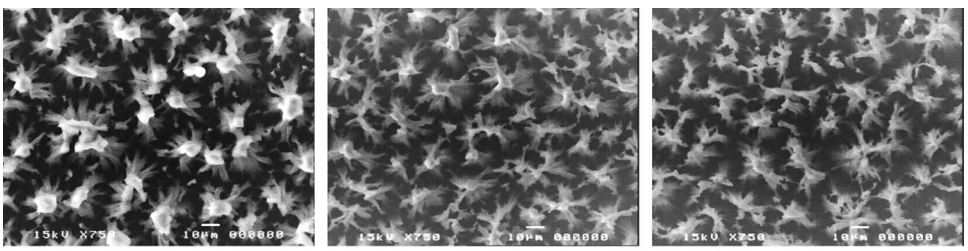

a) 45 mA/cm² *b) 50 mA/cm²* *c) 55 mA/cm²*

Figure 6. Top-view SEM images of needle-like surfaces generated by anodization of <100> CZ 10–20 Ωcm p-type silicon wafers in a 7.2 wt% aqueous solution with various constant current densities in the transition region for 40 minutes.

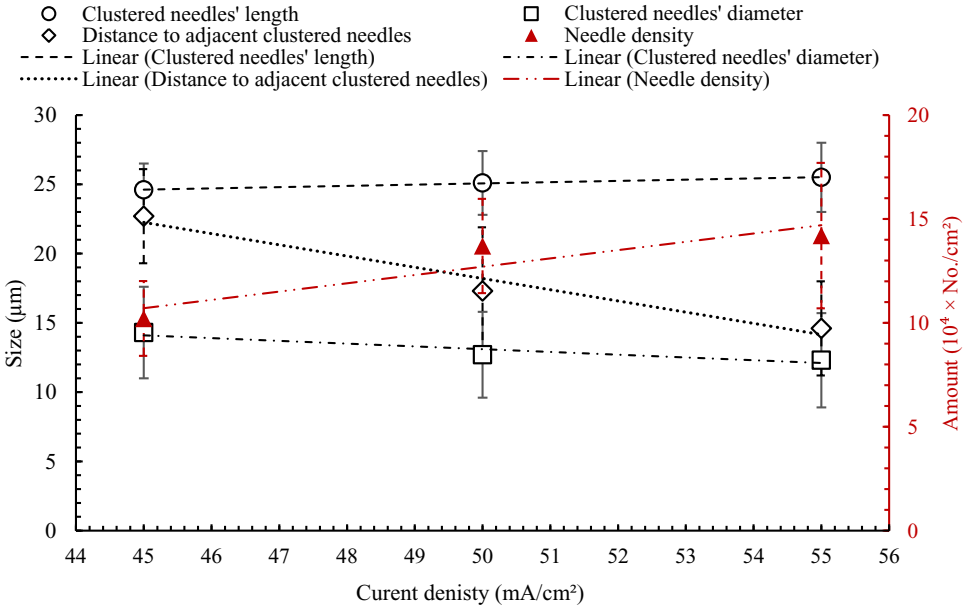

Figure 7. Impact of current density on needle density and geometries of needles generated by anodic etching of <100> CZ 10–20 Ωcm p-type Si wafers in a 7.2 wt% aqueous HF solution for a duration of 40 minutes.

from the15–20 Ωcm wafer had covered by an additional flat surface (probably by a thin micro/meso-pores layer) at the top (Fig. 3c). Needle density and homogeneity of needles were higher in the needle-like surface obtained from the 10–15 Ωcm wafer compared with the one obtained from the 15–20 Ωcm wafer. However, length of needles in the 15–20 Ωcm wafer was a little bit larger than the one obtained from the 10–15 Ωcm wafer.

Impact of electrolyte additive on morphology of needle-like surfaces.—To achieve uniform pore formation, and consequently uniform needle-like surfaces, a surfactant agent like ethanol was added to the aqueous HF electrolyte to diminish the hydrogen bubble formation at silicon/electrolyte interface and to allow full infiltration of the electrolyte into pores.[20] For this purpose, 4-inch <100> CZ 10–20 Ωcm p-type Si wafers with back side sheet resistances of 18.1 ± 0.4 Ω/□ were anodized in 7.2 wt% aqueous HF solutions containing 5 wt% and 15 wt% ethanol with different constant current densities in a range of 20–40 mA/cm^2 for a fixed duration of 40 minutes. The solution containing 15 wt% ethanol resulted in complete electropolishing for all applied constant current densities. The solution containing 5 wt% ethanol resulted only in mountain-like structures (height <10 µm) with different shapes and sizes. These showed that using ethanol as surfactant agent bans the needle formation. This could be due to changes in the electrolyte properties (e.g., conductivity or viscosity) and the semiconductor/electrolyte interface,[21] which varied dissolution kinetics through improved/worsened passivation kinetics;[14] thereby, prohibited the needle formation.

Modeling Formation Mechanisms of Needles in the Transition Region in Respect to Pore Formation Models

During anodic etching of Si in a double tank cell electrochemical setup, the Si is acting as the anode. The current flow between the

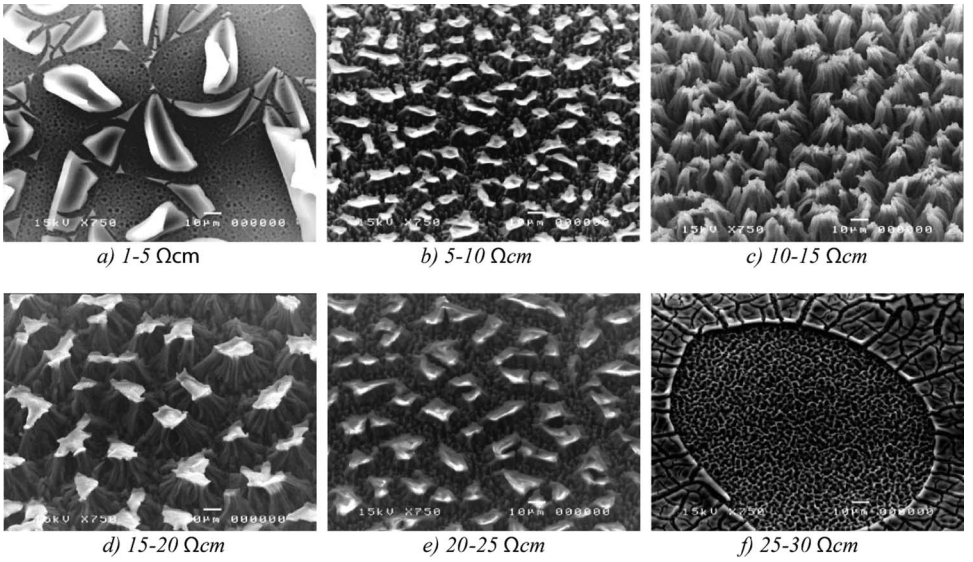

Figure 8. SEM images of surfaces obtained from anodization of <100> CZ p-type silicon wafers with different resistivity values in the lowly doped region in a 7.2 wt% aqueous solution with a constant current density of 50 mA/cm^2 for 40 minutes.

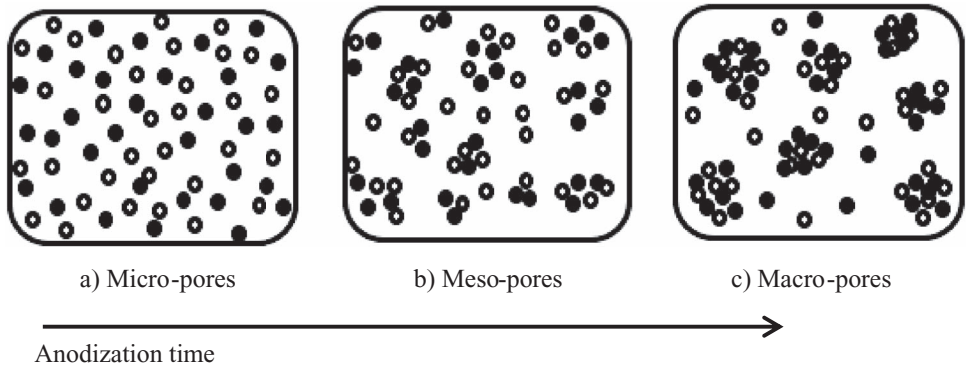

Figure 9. Formation of pores due to correlation of current bursts in time. Time is increasing from left to right. Black dot: active current bursts and hallow circles: inactive current bursts which dissolve oxide bumps (retrieved from[3]).

cathode and the anode releases free holes from the Si-surface to the electrolyte. Arrival of a hole at the Si-electrolyte interface leads to breaking of a Si-Si bond and injection of an electron under certain circumstances, e.g., by ripping off a second bond.[11] In the case of anodic etching of Si in an aqueous HF solution, following chemical reactions may occur:[22]

$$Si + 2F_{ad}^{-} + xh^{+} \rightarrow SiF_2 + (2-x)e^{-} \ (x < 2) \quad [2]$$

$$Si + 4OH_{ad}^{-} + xh^{+} \rightarrow SiO_2 + 2H_2O + (4-x)e^{-} \ (x < 4) \quad [3]$$

$$SiO_2 + 6HF \rightarrow H_2SiF_6 + 2H_2O \quad [4]$$

$$SiF_4 + 2HF \rightarrow H_2SiF_6 \quad [5]$$

where OH_{ad}^{-} and F_{ad}^{-} are adsorbed ions, h^{+} and e^{-} are representing holes and electrons respectively, and x is a coefficient.

All above reactions may proceed on the Si-surface and might compete in rate and coverage of the surface area. The reaction described by Eq. 2 leads to the direct (divalent) dissolution of silicon and requires charge transfer of two electrons (valence number of 2). However, the reaction described by Eq. 3 leads to oxide formation and involves charge transfer of four electrons (valence number of 4). The formed silicon oxide is not stable in the HF-based solution and dissolves according to the reaction described by Eq. 4. This reaction is purely a chemical reaction process and does not involve any charge transfer. The combination of reactions described by Eq. 3 and Eq. 4 describe the indirect (tetravalent) dissolution of silicon via oxidation.[15] Oxide free surfaces are fluorine terminated and tend to be totally covered by hydrogen (H-termination, the reaction based on Eq. 5) if no other reactions take place. H-terminated Si surfaces are then passivated against further dissolution in a relative way.

Above reactions describe only chemical reactions occurring during the anodic etching of Si in an aqueous HF solution. However, nucleation and growth of macro-pores and formation of islets during generation of needles can be explained through the current burst model[11] using above reactions with following major hypothesizes: i) charge transfer and hence current flow is essentially inhomogeneous in space (x, y) and time (t). This means there are times when no charge is transferred in some area at some time. A charge transfer process nucleates at (x, y, t) on the Si surface (or through a thin oxide) with a certain probability, which depends mainly on the state (S) of the surface at (x, y, t). The sequence of events occurring in this way is called a "current burst".[11] ii) The sequence of events in a current burst is logically ordered. It begins with the direct dissolution, followed by oxidation, followed by oxide dissolution, and if a new current burst does not immediately nucleate at the same spot, followed by hydrogen passivation.[11] iii) individual current bursts may interact in space and time. This means the nucleation probability of a current burst is not only a function of the surface state S (x, y, t), but it may also depend on what has happened before at (x, y), interaction in time, or on what is going on in the neighborhood at (t), interaction in space.[11]

In general, a certain amount of Si-dissolution occurs prior to and during initiation of pores.[22] Such an etched layer before pores' initiation is involved in all types of PS since the etching, which causes roughening of the surface, is required for pores initiations.[23,24] Under conditions, where current is relatively large (near J_{PS}) and the direct dissolution is dominant, each individual current burst generates a nm-sized pore by the direct dissolution and oxide removal.[11] Anti-correlation of current bursts in time is then resulting in formation of micro-pores (see Fig. 9a). This means wherever a current burst has stopped, it is less likely that a new current burst will nucleate on the same spot in a short time after. On the other hand, a new current burst nucleates somewhere else (most likely between some former bursts, where the oxide was thinnest).[15] When the current exceeds J_{PS}, current bursts begin to correlate positively in time. This means that likelihood of nucleation of a new current burst in the place, where an old one had occurred, is increased and current bursts begin to cluster. The clustered current bursts are then resulting in formation of either meso-pores or macro-pores (see Figs. 9b and 9c) depending on density of current burst events in a particular area, correlation in space.[25]

In a condition, where the oxidation reaction is low (e.g., in a water free electrolyte), current bursts result in macro-pores covered with meso-porous (transition layer) with a strong preferential growth of both pore types in <100> direction since no oxidation reaction removes the left-over Si between current lines.[26] However, in a condition, where the oxidation reaction is dominant (e.g., in an aqueous electrolyte), oxidation takes over current bursts and smooths the area. This results in macro-pores with no meso-pores coverage (complete dissolution of the transition layer).[27] A transition layer is almost formed in all n-type silicon (with different doping concentrations) and its thickness layer is related to the size of pores: the larger the pores the thicker the transition layer surface. However, for p-type Si, it is found to be only formed in lowly doped substrates.[16] In the transition region, the surface is not completely covered by oxide; therefore, both inhomogeneous and homogenous dissolutions may occur on different regions of the surface.[22] This may result in inhomogeneous dissolution of the transition layer and formation of small islets (remaining bulk Si in the transition layer) above macro-pores at certain times during the anodic etching. With increasing time, the transition layer dissolves entirely and gives access to underneath macro-pores, which have already widened and overlapped. Widening and overlapping of macro-pores may occur due to comparable dissolution rates occurring at the edge of a pore bottom due to current density J_b and at the pore tip due to current density J_t resulting from current density variation and coverage of silicon oxide on the surface of the pore bottom

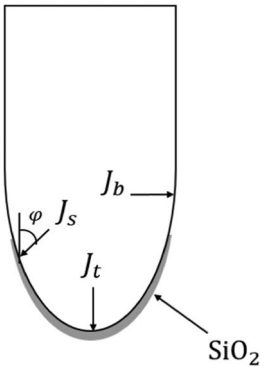

Figure 10. Current variation and coverage of silicon oxide on surface of a pore bottom (retrieved from[1]).

(see Fig. 10) according to:[22]

$$J_s = J_t \cos\varphi + J_b \quad [6]$$

where J_s is the current density on the pore bottom. It is the largest at the pore tip where $\varphi = 0$ and is the smallest on the boundary of the pore bottom where $\varphi = 90$.

This causes a substantial dissolution at the edge of the pore bottom before further propagation of the pore tip and results in complete dissolution of the wall between pores (widening or overlapping of pores).[16] The remaining bulk Si between widened and overlapped macro-pores then result in large irregular islets (see Fig. 11) in which their sizes are larger than the space charge region length – *SCRL* described by:[28]

$$SCRL = \sqrt{\frac{2K\varepsilon\,(V_b - V_a)}{eN_A}} \quad [7]$$

where V_b and V_a are the built-in and the applied potential ($V_a = 0$ at zero current), respectively, $N_A = 7.7 \times 10^{14}$ to 1×10^{15} atoms/cm^3 is the acceptor concentration for (12–17) Ωcm p-type Si, $K = 11.8$ is the Si dielectric constant at 300 K, $\varepsilon = 8.85 \times 10^{-14}$ F/cm is the permittivity of free space, and $e = 1.602 \times 10^{-19}$ C is the elementary charge. The built-in potential (V_b) at the interface of Si can be obtained from:[28]

$$V_b = \frac{E_G}{2e} + \frac{kT}{e} ln\left(\frac{N_A}{n_i}\right) \quad [8]$$

where $E_G = 1.12$ eV is the Si bandgap, $k = 8.617 \times 10^{-5}$ eV/K is the Boltzmann constant, T is the absolute temperature (here 300 K), and $n_i = 1 \times 10^{10}$/cm^3 is the intrinsic concentration of Si at 300 K.

Assuming formed large islets with diameters or widths of ~4.5 ± 1.4 μm (measured from Fig. 3d) as remaining and surrounding walls of widened and overlapped macro-pores in which their thicknesses are almost 3 to 4 times larger than *SCRL* (1 – 1.2 μm for 12–17 Ωcm p-type Si, calculated using Eq. 7), the Lehmann macro-pore

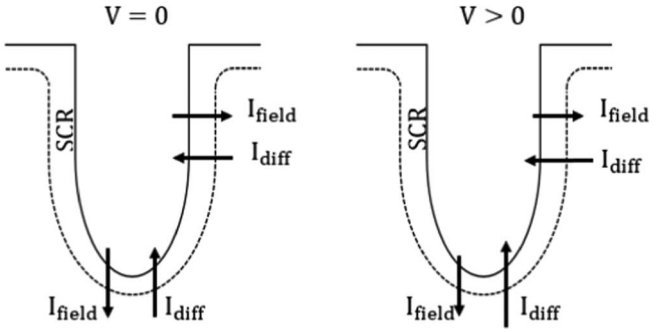

Figure 12. Left: equilibrium (V = 0, equal field and diffusion currents across the space charge region for a macro-pore in p-type Si. Right: reduced field currents under forward bias (V > 0). Note that due to geometric field enhancement at the pore tip, the current at the pore tip is always larger than at the pore walls (retrieved from[2]).

formation model[17] can be used to describe growth of vicinity of pores and reshaping of islets (etching their side walls) to needles. In lowly doped p-type Si, space charge region is not fully depleted of holes at zero bias and under forward conditions.[17] Hence, a diffusion current (I_{diff}) exists at the pore tip and at walls resulting from the concentration gradient of holes, according to the Schottky's theory.[19] At thermal equilibrium and zero applied bias, the I_{diff} is compensated by a field current (I_{field}) as it is shown in Figure 12. Absolute values of the I_{diff} and the I_{field} at the pore tip are larger compared with ones at pore walls since the concentration gradient of holes and electric field strength increases with decreasing the *SCRL*. When a forward bias voltage is applied, the I_{field} decreases while the I_{diff} increases. Hence, higher absolute current values at the pore tip become decisive, and total current at the pore tip ($I_{tip} = (I_{diff} - I_{field})_{tip}$) becomes larger than the current at the pore walls ($I_{wall} = (I_{diff} - I_{field})_{wall}$). As a result, etch rate at the pore tip becomes higher than the etch rate at the pore wall, and consequently the pore tip develops faster than the pore width. However, when thickness of the pore wall reaches a value corresponding to twice of the space charge region length *(2 × SCRL)*, the pore wall is passivated due to depletion of holes in the space charge region. At this stage, only pores tips will develop by further etching of the surface.[17] Hence, with increasing etch time, when diameters of remaining bulk Si between widened pores (islets) reach to 2–2.4 μm *(*twice the *SCRL)* due to further etching of their side walls, islets which have narrowed and reshaped to needles, become passivated. At this stage, further etching does not affect passivated needles, and it develops only tips of their vicinity pores, and consequently increases length of needles. These characteristics can be easily observed from Fig. 13, where a single needle with diameter of about 2.4 μm (almost twice the *SCRL*, 1.87–2.6 μm for 10–20 Ωcm p-type Si) and length of about 25 μm is bent, stretched, and attached to other needles from top.

Impact of current density on morphology of needle-like surfaces and properties of needles can be also explained qualitatively by the

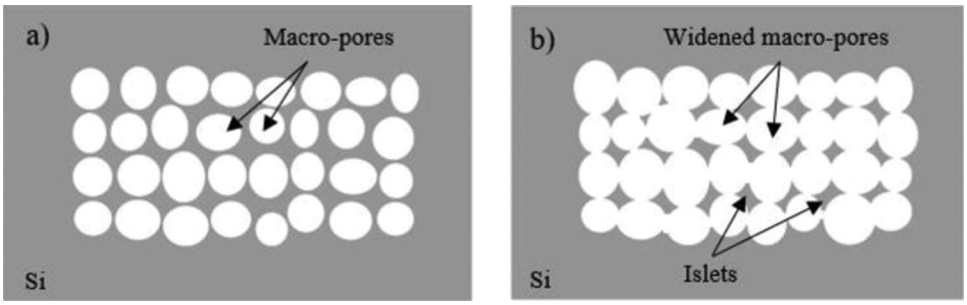

Figure 11. Formation of irregular islets: a) top view of randomly distributed macro-pores with different sizes and pitches and b) top view of widened and overlapped macro-pores, where the remaining bulk Si between them result in irregular islets.

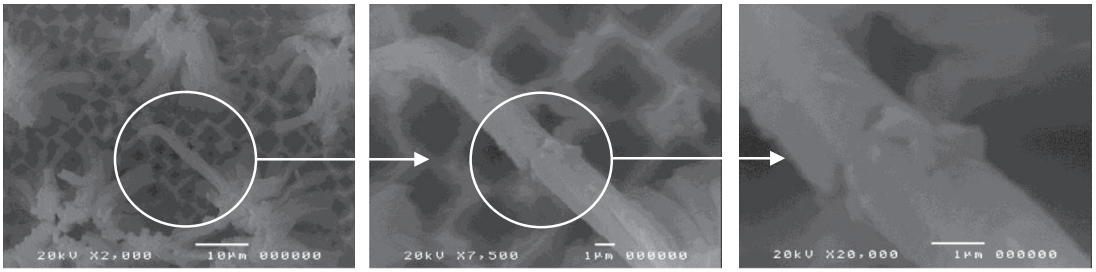

Figure 13. A single needle with diameter of ~2.4 µm (2 × *SCRL* = 1.87–2.6 µm) and length of ~25 µm bent, stretched, and attached to other needles from top. Anodization parameters: current density = 70 mA/cm^2, substrate = 10–20 Ωcm <100> CZ p-type Si, electrolyte = 7.2 wt% aqueous HF, and anodization time = 40 minutes.

current burst model.[11] Increasing current density increases etch rate and number of current bursts events and possibility of their clustering events (interaction in space). This results in formation of more and smaller macro-pores on the Si surface, and consequently larger number of irregular islets with smaller distances between them. This can explain the increase in clustered needle density and the decrease in distance between adjacent clustered needles with increasing current density. In addition, due to higher etch rates at larger current densities, formation and passivation of needles occur earlier and tips of surrounding pores develop faster and for a longer time for a fixed anodization time. These can explain the increase in length of needles and the slight decrease in diameter of clustered needles by increasing current density.

Conclusions

Generation of Si needle-like surfaces by anodic etching of lowly doped p-type Si wafers in an aqueous HF solution in the transition region, where both pore formation and electropolishing compete for control over the surface morphology, is experimentally demonstrated. Formation mechanisms of needles in such surfaces is studied through SEM images taken from surface of wafers after various etch times. A simple model based on pore formation models is presented to describe formation of needles in the transition region for this specific condition. Nucleation of pores and formation of irregular islets (remaining bulk Si between widened and overlapped macro-pores) are explained by the current burst and the Zhang pore formation models. The formation of needles by further etching of side walls of irregular islets and their vicinity pores are described by the Lehmann macro-pore formation model. The model is validated in comparison with experimental results. Effect of electrolyte additives (e.g., ethanol) on morphology of needle-like surfaces are also investigated. Addition of ethanol to the aqueous HF electrolyte changes the conductivity and the viscosity of the electrolyte and the semiconductor/electrolyte interface. This varied dissolution kinetics and prohibited the needle formation. Additionally, impact of current density in the transition region on morphology of needle-like surfaces and properties of needles is studied. Morphology of a needle-like surface and geometrical properties of needles are related to the applied current density. In the case of aqueous HF solution, for a particular wafer resistivity range, HF concentration, and fixed anodization time, clustered needle density and length of clustered needles increase with increasing current density. However, diameter of clustered needles and distance between adjacent clustered needles decrease slightly with increasing current density.

Acknowledgments

The authors thank the Ministry of Science, Research, and Art at the state of Baden-Württemberg, Germany for providing the financial support in the framework program of "Corporative Doctoral Program for Generation Mechanisms of Microstructures - GENMIK."

ORCID

Shervin Keshavarzi https://orcid.org/0000-0002-2003-6700

References

1. P. Kleimann, J. Linnros, and R. Juhasz, *Appl. Phys. Lett.*, **79**(11), 1727 (2001).
2. P. Steiner and W. Lang, *Thin Solid Films*, **255**(1-2), 52 (1995).
3. P. Jonnalagadda, U. Mescheder, A. Kovacs, and A. Nimoe, *Phys. Status Solidi C*, **8**(6), 1841 (2011).
4. S. Keshavarzi, U. Mescheder, and H. Reinecke, *J. Microelectromech. Syst.*, **25**(2), 371 (2016).
5. S. Keshavarzi, U. Mescheder, and H. Reinecke, *J. Microelectromech. Syst.*, **26**(2), 385 (2017).
6. Y. Nishijima, R. Komatsu, S. Ota, G. Seniutinas, A. Balčytis, and S. Juodkazis, *APL Photonics*, **1**(7), 76104 (2016).
7. M. Malekmohammad, M. Soltanolkotabi, A. Erfanian, R. Asadi, S. Bagheri, M. Zahedinejad, M. Khaje, and M. H. Naderi, *JEOS:RP*, **7** (2012).
8. H.-C. Liu and G.-J. Wang, *International Journal of Photoenergy*, **2014**(3), 1–8 (2014).
9. J. Yang, F. Luo, T. S. Kao, X. Li, G. W. Ho, J. Teng, X. Luo, and M. Hong, *Light Sci Appl*, **3**(7), e185 (2014).
10. D. Losic and A. Santos, *Electrochemically engineered nanoporous materials: Methods, properties and applications*, Cham, Springer (2015).
11. H. Föll, M. Christophersen, J. Carstensen, and G. Hasse, *Materials Science and Engineering: R: Reports*, **39**(4), 93 (2002).
12. H. Harada, Y. Mitarai, A. Nishida, M. Miyakoda, and J. Mishima, *Jpn. J. Appl. Phys.*, **43**(5A), 2467 (2004).
13. J. E. A. M. van den Meerakker, R. J. G. Elfrink, W. M. Weeda, and F. Roozeboom, *phys. stat. sol. (a)*, **197**(1), 57 (2003).
14. G. S. Korotchenkov, Editor, *Porous silicon: Formation and properties; Volume one*, Boca Raton, Florida, London, England, New York, CRC Press (2016).
15. H. Föll, M. Leisner, A. Cojocaru, and J. Carstensen, *Materials*, **3**(5), 3006 (2010).
16. X. G. Zhang, *J. Electrochem. Soc.*, **151**(1), C69 (2004).
17. V. Lehmann, *J. Electrochem. Soc.*, **146**(8), 2968 (1999).
18. L. Canham, Editor, *Properties of porous silicon*, London (1997).
19. V. Lehmann, *Electrochemistry of Silicon: Instrumentation, Science, Materials and Applications*, Weinheim, Wiley-VCH (2002).
20. A. Halimaoui, *Appl. Phys. Lett.*, **63**(9), 1264 (1993).
21. T. Defforge, M. Diatta, D. Valente, F. Tran-Van, and G. Gautier, *Journal of the Electrochemical Society*, **160**(4), H247 (2013).
22. X. G. Zhang, *J. Electrochem. Soc.*, **136**(5), 1561 (1989).
23. P. Schmuki, Editor, *Pits and pores II: Formation, properties, and significance for advanced materials; proceedings of the international symposium*, Pennington, NJ, Electrochemical Society (2001).
24. C. Jäger, B. Finkenberger, W. Jäger, M. Christophersen, J. Carstensen, and H. Föll, *Materials Science and Engineering: B*, **69–70**, 199 (2000).
25. J. Carstensen, M. Christophersen, and H. Föll, *Materials Science and Engineering: B*, **69–70**, 23 (2000).
26. X. G. Zhang, *Electrochemistry of Silicon and Its Oxide*, Boston, MA, Kluwer Academic Publishers (2004).
27. C. G. Vayenas, M. E. Gamboa-Adelco, and R. E. White, Editors, *Modern Aspects of Electrochemistry*, Boston, MA, Springer Science+Business Media LLC (2006).
28. R. F. Pierret, *Semiconductor device fundamentals*, Addison-Wesley (1996).